Polymer 50 (2009) 4270–4280

Contents lists available at ScienceDirect

Polymer

journal homepage: www.elsevier.com/locate/polymer

Study of morphology and phase diagram of the H-shaped (AC)B(CA) ternary block copolymers using self-consistent field theory

De-Wen Sun, Zhao-Yan Sun*, Hong-Fei Li, Li-Jia An**

State Key Laboratory of Polymer Physics and Chemistry, Changchun Institute of Applied Chemistry, Chinese Academy of Sciences, Changchun 130022, PR China

ARTICLE INFO

Article history:
Received 16 March 2009
Received in revised form
26 June 2009
Accepted 30 June 2009
Available online 4 July 2009

Keywords:
H-shaped (AC)B(CA) ternary block copolymer
Self-consistent field theory
Phase diagram

ABSTRACT

By using a combinatorial screening method based on the self-consistent field theory (SCFT) for polymer systems, the micro-phase morphologies of the H-shaped (AC)B(CA) ternary block copolymer system are studied in three-dimensional (3D) space. By systematically varying the volume fractions of the components A, B, and C, six triangle phase diagrams of this H-shaped (AC)B(CA) ternary block copolymer system with equal interaction energies among the three components are constructed from the weaker segregation regime to the strong segregation regime. In this study, thirteen 3D micro-phase morphologies for this H-shaped ternary block copolymer system are identified to be stable and seven 3D micro-phase morphologies are found to be metastable. It is found that in the weaker segregation regime ($\chi_{AB}N = \chi_{AC}N = \chi_{BC}N = 45$), the minority component can be mixed with other two majority components to form the mixed phase regions, while in the intermediate segregation regime ($\chi_{AB}N = \chi_{AC}N = \chi_{BC}N = 60$ and 75), the mixed phase regions phase-separate into three distinct phase regions. In the strong segregation regime ($\chi_{AB}N = \chi_{AC}N = \chi_{BC}N = 90$, 100, and 125), the distinct blocks tend to separate with each other and the phase behavior of this H-shaped (AC)B(CA) ternary block copolymer is similar to that of the three-arm star-like ABC ternary block copolymer. Moreover, the order–disorder transitions and the order–order transitions by varying the interaction parameters are discussed. These results may help in the design of the microstructures of complex block copolymers.

1. Introduction

It is well known that block copolymers have fascinating ability to self-assemble into a variety of ordered micro-phase morphologies on nanometer scale [1] due to their particular chemical structures and smart balance between the interfacial energy and conformational entropy. Block copolymers have attracted a great deal of attention both theoretically and experimentally because of their wide applications in many fields, such as nano-scale colloidal particles [2], surface patterning [3], and the creation of photonic band-gap materials [4]. It has been demonstrated by both theories and experiments that the micro-phase morphologies of block copolymers depend on not only the compositions and interaction energies between distinct components but also the particular chain architectures. With the development of synthetic methods, block copolymers with more complex chain architectures, such as π-shaped [5], H-shaped [6–10], dendrimer-like [8], comb-like [11], barbwire-like [11], centipede-like [11–13], and core cross-linked star-like [14] polymers, have been synthesized, which makes it possible to study the effect of molecular architectures on the micro-phase behavior of block copolymers in detail.

An H-shaped (AC)B(CA) ternary block copolymer has four side-arms (A1, C1, A2, C2) attached to the end of the backbone (B), where A1 arm and C1 arm are at one end while A2 arm and C2 arm at the other end. A schematic representation of the architecture is shown in Fig. 1. This ternary block copolymer may have some important applications in the fields such as controlled drug delivery, macromolecular self-assembly, and the preparation of advanced materials [8]. However, it is difficult to obtain the phase diagrams and predict the micro-phase separation behavior in experiment because of the complexity of synthesizing block copolymers with different chain architectures. Therefore, it is important to predict the micro-phase morphologies and phase behavior of this H-shaped (AC)B(CA) ternary block copolymer theoretically.

The self-consistent field theory (SCFT) [15–26] has been proved to be one of the most accurate mean-field theories to study the phase behavior of polymeric complex fluids. Several efficient numerical methods have been established to solve the SCFT equations. In 1994, the spectral method, i.e., the reciprocal space

* Corresponding author. Tel.: +86 431 85262896; fax: +86 431 85262969.
** Corresponding author. Tel.: +86 431 85262988; fax: +86 431 85685653.
E-mail addresses: zysun@ciac.jl.cn (Z.-Y. Sun), ljan@ciac.jl.cn (L.-J. An).

0032-3861/$ – see front matter
doi:10.1016/j.polymer.2009.06.072

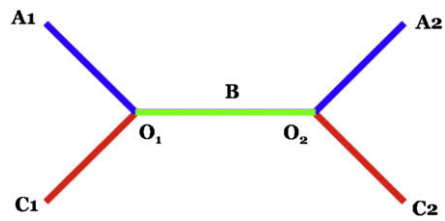

Fig. 1. Molecular architectures of H-shaped (AC)B(CA) ternary block copolymer.

method, was proposed by Matsen and Schick [19], which is suitable and effective in constructing the phase diagrams due to its precise computation of free energy and numerical efficiency. The spectral method can be carried out by using the previously assumed ordered micro-phase morphologies [19] or using the general basis functions [20]. In 1999, Drolet and Fredrickson [21–23] developed the combinatorial screening method, i.e., the real space method. The real space method does not require the prior symmetry information of the previously unknown micro-phase morphologies and the numerical implementation of SCFT equations is performed in real space in an adaptive arbitrary cell. Therefore, this method can be employed to study the previously unknown complex micro-phase morphologies. In 2002, Tzeremes et al. proposed the pseudo-spectral method, which also requires no prior knowledge of symmetry and can improve the efficiency of calculations [24]. One year later, Fredrickson et al. proposed a parallel algorithm for numerical self-consistent field theory simulations of block copolymer structures based on this pseudo-spectral method in order to implement large-cell calculations [25]. Very recently, a new reciprocal method, i.e., the generic Fourier-space approach, has been proposed by Guo et al. [26] to discover the ordered micro-phase morphologies of block copolymers. This method is based on the fact that all the spatially varying functions are spanned by the Fourier series determined by the size and shape of the box for any computational box with periodic boundary conditions [26].

With the development of simulation method, a large number of theoretical works have been done to explore the complex micro-phase morphologies and phase behaviors of these complex block copolymers [27–33]. However, for the sake of numerical tractability, most of these theoretical implementations were carried out in two-dimensional (2D) space. Although 2D studies can investigate the micro-phase morphologies with translational invariance along certain directions, such as lamellar and cylindrical structures, a great deal of information of three-dimensional (3D) intrinsic micro-phase morphologies, such as the double gyroid, double-diamond, and spherical structures, cannot be predicted. Therefore, in order to describe the phase behavior of block copolymers in detail, 3D studies are very necessary. Recently, Sun et al. have studied the 3D micro-phase morphologies and obtained one-dimensional (1D) phase diagrams of the linear ABC ternary block copolymer system via SCFT [34].

In this study, the combinatorial screening method is used to study the 3D micro-phase morphologies of this H-shaped (AC)B(CA) ternary block copolymer and the triangle phase diagrams are obtained. Furthermore, the influences of the compositions and the interaction energies between distinct components on the micro-phase separation behavior have been investigated through these 3D micro-phase morphologies and triangle phase diagrams.

2. Theoretical method

We consider a melt consisting of n H-shaped (AC)B(CA) ternary block copolymers. Each polymer is composed of N segments, and the blocks A, B, and C have f_AN, f_BN, and f_CN monomers, respectively. As shown in Fig. 1, this H-shaped ternary block copolymer can be divided into five parts. The free energy of this system is given by

$$\begin{aligned}\frac{F}{nk_BT} = & -\ln\left(\frac{Q}{V}\right) + \frac{1}{V}\int \mathrm{d}\mathbf{r}\{\chi_{AB}N[\varphi_A(\mathbf{r}) - f_A][\varphi_B(\mathbf{r}) - f_B] \\ & + \chi_{AC}N[\varphi_A(\mathbf{r}) - f_A][\varphi_C(\mathbf{r}) - f_C] + \chi_{BC}N[\varphi_B(\mathbf{r}) - f_B][\varphi_C(\mathbf{r}) \\ & - f_C] - \omega_A(\mathbf{r})[\varphi_A(\mathbf{r}) - f_A] - \omega_B(\mathbf{r})[\varphi_B(\mathbf{r}) - f_B] \\ & - \omega_C(\mathbf{r})[\varphi_C(\mathbf{r}) - f_C] - \xi(\mathbf{r})[1 - \varphi_A(\mathbf{r}) - \varphi_B(\mathbf{r}) - \varphi_C(\mathbf{r})]\}\end{aligned} \tag{1}$$

where V is the volume of the system; $\varphi_A(\mathbf{r})$, $\varphi_B(\mathbf{r})$, and $\varphi_C(\mathbf{r})$ are the monomer density fields normalized by the local volume fractions of A, B, and C, respectively; χ_{AB}, χ_{AC}, and χ_{BC} are Flory–Huggins interaction parameters between two different components; $\omega_A(\mathbf{r})$, $\omega_B(\mathbf{r})$, and $\omega_C(\mathbf{r})$ are the self-consistent fields that conjugate to the density fields $\varphi_A(\mathbf{r})$, $\varphi_B(\mathbf{r})$, and $\varphi_C(\mathbf{r})$, respectively; $\xi(\mathbf{r})$ is the potential field that ensures the incompressibility of the system and is also known as a Lagrange multiplier. Minimizing the free energy with respect to $\varphi_A(\mathbf{r})$, $\varphi_B(\mathbf{r})$, $\varphi_C(\mathbf{r})$, $\omega_A(\mathbf{r})$, $\omega_B(\mathbf{r})$, $\omega_C(\mathbf{r})$, and $\xi(\mathbf{r})$ leads to the following SCFT Eqs. (2)–(9) which describe the equilibrium micro-phase morphologies:

$$\omega_A(\mathbf{r}) = \chi_{AB}N[\varphi_B(\mathbf{r}) - f_B] + \chi_{AC}N[\varphi_C(\mathbf{r}) - f_C] + \xi(\mathbf{r}) \tag{2}$$

$$\omega_B(\mathbf{r}) = \chi_{AB}N[\varphi_A(\mathbf{r}) - f_A] + \chi_{BC}N[\varphi_C(\mathbf{r}) - f_C] + \xi(\mathbf{r}) \tag{3}$$

$$\omega_C(\mathbf{r}) = \chi_{AC}N[\varphi_A(\mathbf{r}) - f_A] + \chi_{BC}N[\varphi_B(\mathbf{r}) - f_B] + \xi(\mathbf{r}) \tag{4}$$

$$\varphi_A(\mathbf{r}) + \varphi_B(\mathbf{r}) + \varphi_C(\mathbf{r}) = 1 \tag{5}$$

$$\begin{aligned}\varphi_A(\mathbf{r}) = & \frac{V}{Q}\int_0^{f_{A1}} \mathrm{d}s q_{A10}(\mathbf{r},s)q_{A11}(\mathbf{r},f_{A1} - s) \\ & + \frac{V}{Q}\int_0^{f_{A2}} \mathrm{d}s q_{A20}(\mathbf{r},s)q_{A21}(\mathbf{r},f_{A2} - s)\end{aligned} \tag{6}$$

$$\varphi_B(\mathbf{r}) = \frac{V}{Q}\int_0^{f_B} \mathrm{d}s q_{B0}(\mathbf{r},s)q_{B1}(\mathbf{r},f_B - s) \tag{7}$$

$$\begin{aligned}\varphi_C(\mathbf{r}) = & \frac{V}{Q}\int_0^{f_{C1}} \mathrm{d}s q_{C10}(\mathbf{r},s)q_{C11}(\mathbf{r},f_{C1} - s) \\ & + \frac{V}{Q}\int_0^{f_{C2}} \mathrm{d}s q_{C20}(\mathbf{r},s)q_{C21}(\mathbf{r},f_{C2} - s)\end{aligned} \tag{8}$$

$$Q = \int \mathrm{d}\mathbf{r} q_{\alpha 0}(\mathbf{r},s)q_{\alpha 1}(\mathbf{r},f_\alpha - s) \tag{9}$$

where Q is the partition function of a single chain in the effective fields $\omega_A(\mathbf{r})$, $\omega_B(\mathbf{r})$, and $\omega_C(\mathbf{r})$. $q_{\alpha\beta}(\mathbf{r},s)$, where $\alpha = $ A1, A2, B, C1, C2, and $\beta = 0, 1$, is the polymer segment probability distribution function, which gives the probability of finding segment s at position $\mathbf{r}$ and satisfies the modified diffusion equation (Eq. (10)). $\beta = 0$ corresponds to s of $q_{\alpha\beta}(\mathbf{r},s)$ increasing from the free end to the nearer point (O_1 or O_2) or from point O_1 to point O_2, and $\beta = 1$ corresponds to s of $q_{\alpha\beta}(\mathbf{r},s)$ increasing reversely. It should be noted that Q is independent of the chain contour length parameter s.

The modified diffusion equation reads

$$\frac{\partial q_{\alpha\beta}(\mathbf{r},s)}{\partial s} = \nabla^2 q_{\alpha\beta}(\mathbf{r},s) - \omega_\alpha(\mathbf{r}) q_{\alpha\beta}(\mathbf{r},s) \tag{10}$$

where $0 < s < f_\alpha$. The initial conditions of $q_{\alpha\beta}(\mathbf{r},s)$ are

$$q_{A10}(\mathbf{r},0) = q_{A20}(\mathbf{r},0) = q_{C10}(\mathbf{r},0) = q_{C20}(\mathbf{r},0) = 1.0,$$

$$q_{B0}(\mathbf{r},0) = q_{A10}(\mathbf{r},f_{A1}) q_{C10}(\mathbf{r},f_{C1}),$$

$$q_{B1}(\mathbf{r},0) = q_{A20}(\mathbf{r},f_{A2}) q_{C20}(\mathbf{r},f_{C2}),$$

$$q_{A11}(\mathbf{r},0) = q_{B1}(\mathbf{r},f_B) q_{C10}(\mathbf{r},f_{C1}),$$

$$q_{A21}(\mathbf{r},0) = q_{B0}(\mathbf{r},f_B) q_{C20}(\mathbf{r},f_{C2}),$$

$$q_{C11}(\mathbf{r},0) = q_{B1}(\mathbf{r},f_B) q_{A10}(\mathbf{r},f_{A1}),$$

and

$$q_{C21}(\mathbf{r},0) = q_{B0}(\mathbf{r},f_B) q_{A20}(\mathbf{r},f_{A2}),$$

which are similar to those in References [28–31]. Eq. (10) is solved by the Douglas–Gunn scheme and alternating direction implicit method because the Douglas–Gunn scheme is unconditionally stable in 3D space while the Crank–Nicholson scheme is only conditionally stable in 3D space [35,36].

The Douglas–Gunn scheme for Eq. (10) is

$$\frac{q_{xyz}^{s+1/3} - q_{xyz}^{s}}{\Delta s} = \frac{1}{\Delta^2}\left[\delta_x^2\left(\frac{q_{xyz}^{s+1/3} + q_{xyz}^{s}}{2}\right) + \delta_y^2 q_{xyz}^{s} + \delta_z^2 q_{xyz}^{s}\right] - \frac{1}{2} W_{xyz}\left(q_{xyz}^{s+1/3} + q_{xyz}^{s}\right)$$

$$\frac{q_{xyz}^{s+2/3} - q_{xyz}^{s}}{\Delta s} = \frac{1}{\Delta^2}\left[\delta_x^2\left(\frac{q_{xyz}^{s+1/3} + q_{xyz}^{s}}{2}\right) + \delta_y^2\left(\frac{q_{xyz}^{s+2/3} + q_{xyz}^{s}}{2}\right) + \delta_z^2 q_{xyz}^{s}\right] - \frac{1}{2} W_{xyz}\left(q_{xyz}^{s+2/3} + q_{xyz}^{s}\right)$$

$$\frac{q_{xyz}^{s+1} - q_{xyz}^{s}}{\Delta s} = \frac{1}{\Delta^2}\left[\delta_x^2\left(\frac{q_{xyz}^{s+1/3} + q_{xyz}^{s}}{2}\right) + \delta_y^2\left(\frac{q_{xyz}^{s+2/3} + q_{xyz}^{s}}{2}\right) + \delta_z^2\left(\frac{q_{xyz}^{s+1} + q_{xyz}^{s}}{2}\right)\right] - \frac{1}{2} W_{xyz}\left(q_{xyz}^{s+1} + q_{xyz}^{s}\right)$$

$$\begin{aligned}\delta_x^2 q_{xyz}^{s} &= q_{x+1yz}^{s} - 2q_{xyz}^{s} + q_{x-1yz}^{s}, \delta_y^2 q_{xyz}^{s} \\ &= q_{xy+1z}^{s} - 2q_{xyz}^{s} + q_{xy-1z}^{s}, \delta_z^2 q_{xyz}^{s} \\ &= q_{xyz+1}^{s} - 2q_{xyz}^{s} + q_{xyz-1}^{s}\end{aligned}$$

where Δs is the reciprocal of the chain length N; Δ is lattice spacing and chosen as $\Delta = dx = dy = dz$. Obviously, the Douglas–Gunn scheme only needs to solve cyclic tridiagonal systems at each contour step.

The self-consistent field $\omega_\alpha(\mathbf{r})$ can be updated by using the following equation [21–23]:

$$\omega_\alpha^{\text{new}} = \omega_\alpha^{\text{old}} + \Delta t\left(\frac{\delta F}{\delta \varphi_\alpha}\right)^* \tag{11}$$

where the time step $\Delta t = 0.01$–0.1 and

$$\left(\frac{\delta F}{\delta \varphi_\alpha}\right)^* = \sum_{M \neq \alpha} \chi_{\alpha M} N(\varphi_M - f_M) + \xi - \omega_\alpha^{\text{old}} \tag{12}$$

The above steps are iterated until the free energy converges to a local minimum, which corresponds to a metastable or stable micro-phase structure [27–34]. In our simulations, the iteration terminates when the changes of the self-consistent fields $\omega_\alpha(\mathbf{r})$ are all reduced to 10^{-4}. Each minimization is run several times using different initial random guesses of the self-consistent fields $\omega_\alpha(\mathbf{r})$. During constructing the triangle phase diagrams, we have identified the most stable structure by comparing the free energy when encountering metastable states. It should be noted that one must be careful when two-step transitions occur for ABC ternary block polymers. Upon slow cooling, the traditional "two-color" diblock-type micro-phase morphologies are found first. Then the second one may be constrained from the first micro-phase morphology. Therefore, in our study, when identifying the stability of the "three-color" micro-phase morphologies, we combine the slow-cooling method and the fast-cooling method. First, the fast-cooling method is used to explore the previously unknown micro-phase morphologies. Then the previous domain boundaries of the slow-cooling "two-color" micro-phase morphologies are used to obtain the slow-cooling "three-color" micro-phase morphologies. Then we compare all the saddle point free energies of the slow-cooling and fast-cooling micro-phase morphologies to identify the most stable micro-phase morphology.

The Lagrange multiplier $\xi(\mathbf{r})$ can be obtained by solving Eqs. (2)–(5) [37]:

$$\xi = \frac{C_1C_2(\omega_A + \omega_C) + C_1C_3(\omega_B + \omega_C) + C_2C_3(\omega_A + \omega_B)}{2(C_1C_2 + C_1C_3 + C_2C_3)} \tag{13}$$

where

$$C_1 = -\chi_{AB}N + \chi_{BC}N + \chi_{AC}N,$$

$$C_2 = -\chi_{BC}N + \chi_{AB}N + \chi_{AC}N,$$

$$C_3 = -\chi_{AC}N + \chi_{AB}N + \chi_{BC}N.$$

The implementation of above SCFT equations is carried out in a 3D cubic cell with periodic boundary conditions. The system size is changed from 46^3 to 128^3 in order to avoid the finite-size effects. In this calculation, the system size usually used is 58^3–80^3 and only a few calculations using the system size more than 100^3. The capability of our computers can fulfill the need of calculations and therefore we did not use the parallel algorithm based on the fast Fourier transformation method developed by Fredrickson et al. [25]. In our simulations, the side length of the box $L = V^{1/3}$ is initially chosen as a small one, and then increased until the free energy does not decrease. The chain length of the block copolymers is fixed as $N = 100$. The lattice spacings are chosen as $dx = dy = dz = b/4$, where b is the Kuhn length of the polymer segment. Since the radius of gyration of the polymer chain satisfies $R_g^2 = Nb^2/6$, the side length L is in the range of 2.8–7.85R_g of polymers. Then the free energy of the obtained "equilibrium" structure in the above calculation is minimized with respect to the aspects of the simulation cell.

3. Results and discussions

In this work, the 3D micro-phase morphologies are studied and the triangle phase diagrams are obtained for the H-shaped (AC)B(CA) ternary block copolymers with symmetric interaction parameters, i.e., $\chi_{AB}N = \chi_{AC}N = \chi_{BC}N$. By systematically changing

the volume fractions of the components A, B, and C at each interaction parameter, six three-component triangle phase diagrams in the entire range of the composition are constructed. The increase of the volume fractions f_A, f_B, and f_C in these phase diagrams is 0.1. At each grid point, the most stable micro-phase morphology is obtained by using the approach described in the above section. For convenience, we only consider the system with the same volume fraction of A1 and A2 arms or C1 and C2 arms. It can be seen that all the triangle phase diagrams clearly show the A–C reflection symmetry with symmetric interaction parameters. Three different colors, i.e., blue, green, and red are assigned to represent the components A, B, and C, respectively. Tables 1 and 2 show all the ordered micro-phase morphologies that are found stable and metastable for this H-shaped (AC)B(CA) ternary block copolymer, respectively. Thirteen 3D micro-phase morphologies are identified to be stable, including the body-centered-cubic sphere phase (BCC), the hexagonally packed cylinder phase (HPC), the core–shell hexagonally packed cylinder phase (CSHPC), the "two-color" hexagonally perforated layer phase (HPL_2), the "three-color" hexagonally perforated layer phase (HPL_3), the "two-color" lamellae phase (LAM_2), the "three-color" lamellae phase (LAM_3), the "three-color" hexagonal honeycomb packed cylinder phase (HEX_3-PC), the dodecagon–hexagon–tetragon packed cylinder phase (DOHT-PC), the octagon–hexagon–tetragon packed cylinder phase (OHT-PC), the octagon–octagon–tetragon packed cylinder phase (OOT-PC), the lamellae with alternating cylinders phase (LAM + C), and the lamellae with cylinders inside phase (LAM + C-I), and seven metastable micro-phase morphologies are also observed, including the "two-color" *Fddd*-like network phase (*Fddd*L_2), the "two-color" Diamond-like network phase (DL_2), the "three-color" core–shell *Fddd*-like network phase (CS*Fddd*L_3), the "three-color" core–shell Diamond-like network phase ($CSDL_3$), the decagon–hexagon–tetragon packed cylinder phase (DEHT-PC), the knitting pattern packed cylinder phase (KP-PC), and the simple-cubic spheres connected by cylinders phase (SCS + C). In order to make a clear representation of the final pattern, all the linear dimensions of the unit cell are replicated 2 times in each dimension. In this work, some intrinsic 3D micro-phase morphologies, such as the BCC morphology and the hexagonally perforated layer phase (HPL) morphology, are observed, while these micro-phase morphologies cannot be predicted in 2D studies. In the following sections, we discuss the phase behavior of this H-shaped (AC)B(CA) ternary block copolymer in detail.

3.1. Weaker segregation regime ($\chi_{AB}N = \chi_{AC}N = \chi_{BC}N = 45$)

In the weaker segregation regime, the minority component can be mixed with other two majority components to form the mixed phase regions. Fig. 2 shows the three-component triangle phase diagram which covers the whole range of the block copolymer compositions when $\chi_{AB}N = \chi_{AC}N = \chi_{BC}N = 45$. It should be noted that the interaction parameter $\chi_{AB}N = \chi_{AC}N = \chi_{BC}N = 45$ is not really in the weak segregation regime, but with this interaction parameter, the "two-color" micro-phase morphologies can be observed because the interaction parameters between different blocks are weak enough that the minority component can be mixed with other two majority components to form the mixed phase regions. It can be clearly seen that most of grid points are occupied by the LAM_2 morphology.

Near the two edges (AB and BC) of this triangle phase diagram, the phase behavior is similar to that of the symmetric linear ABA binary block copolymer [38]. With the volume fraction f_B increasing from 0.1 to 0.8, the micro-phase morphologies change from disorder to HPC, HPL_2, LAM_2, BCC, and finally to disorder morphology. Near the AC edge of this triangle phase diagram, the phase behavior is similar to that of the A_2B_2 binary block copolymer [39]. With the volume fraction f_A increasing from 0.1 to 0.8, the micro-phase morphologies change from disorder to HPC, LAM_2, HPC, and finally to disorder. For these "two-color" micro-phase morphologies, the minority component is enriched at the interfaces between other two majority components. This is attributed to the chain architecture of this H-shaped (AC)B(CA) ternary block copolymer, where both ends of the block B are connected by block A and block C.

For the H-shaped (AC)B(CA) ternary block copolymers, when $f_A = f_C$, there is a competition between the compatibility and repulsion of components A and C. When the volume fraction f_B is large, the components A and C can be mixed together. With the volume fraction f_B decreasing from 0.8 to 0.4, the following micro-phase morphologies appear gradually: disorder → BCC → LAM_2 → HPC. When the volume fraction f_B continues decreasing, the components A and C phase-separate with each other and the OOT-PC morphology is observed. It can be seen that the OOT-PC morphology has the translational invariance along certain directions so that the octagon–octagon–tetragon phase (OOT) morphology can be observed in 2D space [28,29]. However, in this weaker segregation regime, some complex 3D intrinsic micro-phase morphologies, such as the "two-color" double gyroid phase (DG) and the "two-color" double-diamond phase (DD), are not observed.

3.2. Intermediate segregation regime ($\chi_{AB}N = \chi_{AC}N = \chi_{BC}N = 60$ and 75)

In the intermediate segregation regime ($\chi_{AB}N = \chi_{AC}N = \chi_{BC}N = 60$ and 75), some previously (at lower χN value) mixed phase regions now start to phase-separate to form three different phase regions. Fig. 3 shows the three-component triangle phase diagrams which cover the whole range of the block copolymer compositions when $\chi_{AB}N = \chi_{AC}N = \chi_{BC}N = 60$ and 75. It can be clearly seen that the stable region of the LAM_2 morphology is greatly reduced.

In the center region of these two triangle phase diagrams (Fig. 3a and b), when the volume fraction $f_B = 0.4$ and other two volume fractions are equal, the OHT-PC morphology is observed. This 3D micro-phase morphology has been observed in the three-arm star-like ABC ternary block copolymers by Gemma et al. using Monte Carlo (MC) simulation [40]. Obviously, the OHT-PC morphology also has the translational invariance along certain directions, which is similar to the OOT-PC morphology. In the stable region of the OHT-PC morphology in this segregation regime, the metastable HEX_3-PC, DEHT-PC, DOHT-PC, and OOT-PC morphologies are observed, which have similar saddle point free energies in this phase region (data not shown). In the OHT-PC morphology, the majority component B forms the octagonal cylinder phase domains, while other two components A and C form their own hexagonal and tetragonal cylinder phase domains, respectively. For the formation of the DOHT-PC morphology, since the majority component B forms the dodecagonal cylinder phase domains, the component A (C) will form the tetragonal cylinder phase domains if the component C (A) forms the hexagonal cylinder phase domains. However, when the volume fraction f_A (f_C) = 0.4 and other two volume fractions are equal, the HEX_3-PC morphology is found to be more stable than the OHT-PC morphology. This is mainly because that in this case the block copolymer has shorter chain length of the bridge block (block B). The HEX_3-PC morphology has also been observed for the three-arm star-like ABC ternary block copolymers by Monte Carlo (MC) simulation [40,41] and dynamic density functional theory (DDFT) study [42]. Due to its translational invariance along certain directions, the "three-color" hexagonal honeycomb phase (HEX_3) morphology can be predicted in 2D space

Table 1
Summary of observed 3D stable micro-phase morphologies.

Name	Abbreviation	Morphology	Graphic
Body-centered-cubic sphere phase	BCC	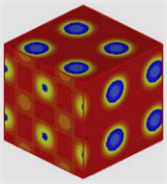	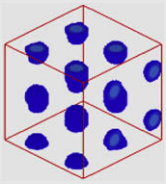
Hexagonally packed cylinder phase	HPC	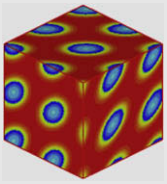	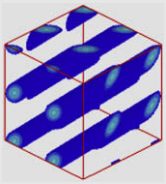
Core–shell hexagonally packed cylinder phase	CSHPC	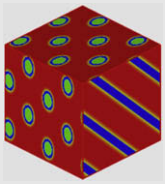	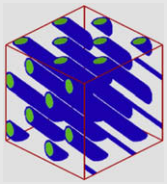
“Two-color” hexagonally perforated layer phase	HPL_2	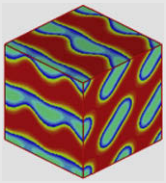	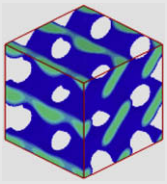
“Three-color” hexagonally perforated layer phase	HPL_3	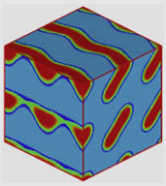	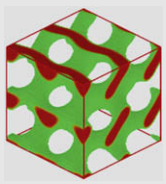
“Two-color” lamellae phase	LAM_2	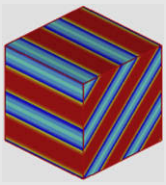	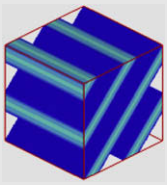
“Three-color” lamellae phase	LAM_3	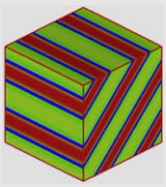	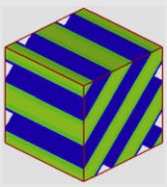

Table 1 (*continued*)

Name	Abbreviation	Morphology	Graphic
"Three-color" hexagonal honeycomb packed cylinder phase	HEX_3-PC	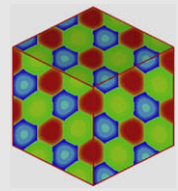	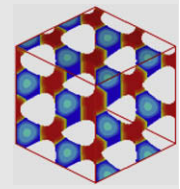
Dodecagon–hexagon–tetragon packed cylinder phase	DOHT-PC	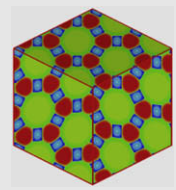	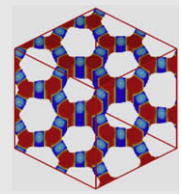
Octagon–hexagon–tetragon packed cylinder phase	OHT-PC	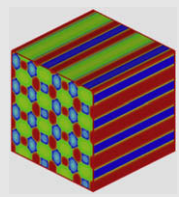	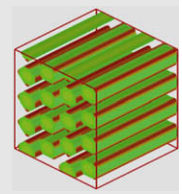
Octagon–octagon–tetragon packed cylinder phase	OOT-PC	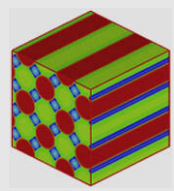	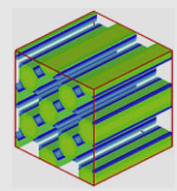
Lamellae with alternating cylinders phase	LAM + C	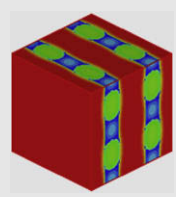	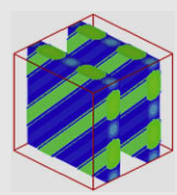
Lamellae with cylinders inside phase	LAM + C-I	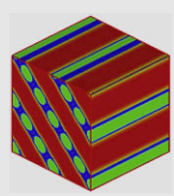	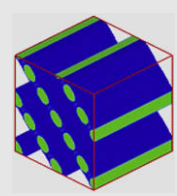

[28,29,43], which is similar to the OOT-PC and OHT-PC morphologies. It should be noted that in the stable region of the HEX_3-PC morphology, the saddle point free energies of the OHT-PC, HEX_3-PC, and OOT-PC morphologies are similar and are all lower than that of the DEHT-PC and DOHT-PC morphologies (data not shown) whose saddle point free energies are also similar.

In these two triangle phase diagrams (Fig. 3a and b), when the volume fraction f_A (f_C) = 0.2, as the volume fraction f_B increases from 0.3 to 0.5, the LAM_3 morphology is observed. For this LAM_3 morphology, the lamellar widths D_A, D_B, and D_C satisfy the following regularity, i.e., D_A:D_B:$D_C \approx f_A$:$2f_B$:$2f_C$ when component A is the minority component while D_A:D_B:$D_C \approx 2f_A$:$2f_B$:f_C when component C is the minority component. However, for the linear ABC ternary block copolymers [27,34], the lamellar widths D_A, D_B, and D_C obey D_A:D_B:$D_C \approx 2f_A$:f_B:$2f_C$. This is due to the difference of the chain architectures of these two block copolymers. Furthermore, these LAM_3 morphologies all follow the CABA sequence. When the volume fraction f_B is small, this sequence implies that most of the chains might adopt the bridge-type configuration. With the increase of the segregation degree (Fig. 3b), in the stable region of the LAM_3 morphology, the metastable KP-PC, OOT-PC, and DOHT-PC morphologies are observed. In KP-PC morphology, the

Table 2
Summary of observed 3D metastable micro-phase morphologies.

Name	Abbreviation	Morphology	Graphic
"Two-color" *Fddd*-like network phase	*Fddd*L_2	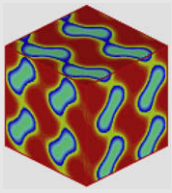	
"Two-color" Diamond-like network phase	DL_2	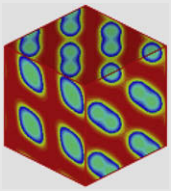	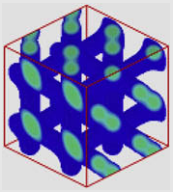
"Three-color" core–shell *Fddd*-like network phase	CS*Fddd*L_3	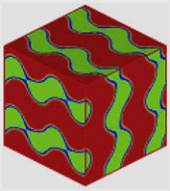	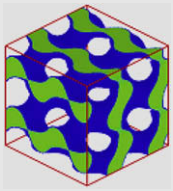
"Three-color" core–shell Diamond-like network phase	$CSDL_3$	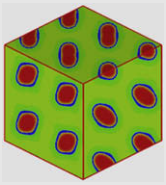	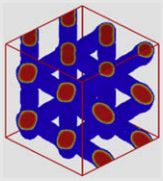
Decagon–hexagon–tetragon packed cylinder phase	DEHT-PC	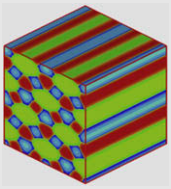	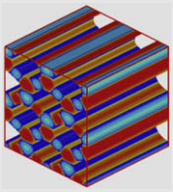
Knitting pattern packed cylinder phase	KP-PC	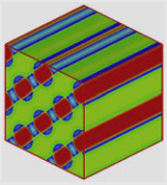	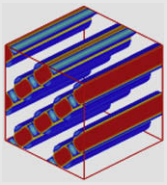
Simple-cubic spheres connected by cylinders phase	SCS + C	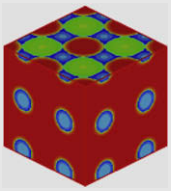	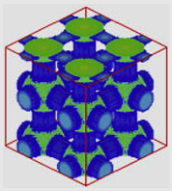

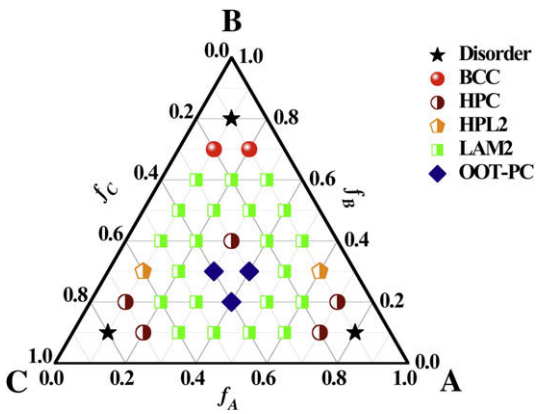

Fig. 2. Triangle phase diagram when $\chi_{AB}N = \chi_{AC}N = \chi_{BC}N = 45$.

two minority components form the knitting patterns, while the majority component fills the left space. For the DOHT-PC morphology, the majority component forms the dodecagonal cylinder phase domains and the minority component forms the tetragonal cylinder phase domains, which is different from that when $f_A/f_B/f_C$ is 0.3/0.4/0.3. Moreover, in the OOT-PC morphology, the two majority components form the octagonal cylinder phase domains while the minority component forms the tetragonal phase domains. The saddle point free energies for LAM_3, KP-PC, OOT-PC, and DOHT morphologies for three different compositions are listed in Table 3 when $f_A = 0.2$ and $\chi_{AB}N = \chi_{AC}N = \chi_{BC}N = 75$. It can be seen

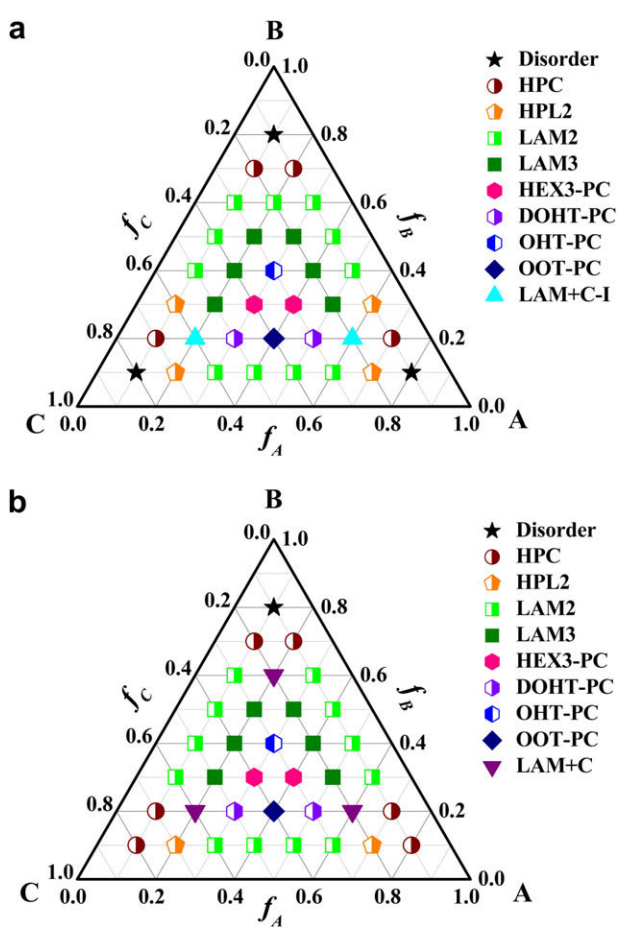

Fig. 3. Triangle phase diagram for the system with (a) $\chi_{AB}N = \chi_{AC}N = \chi_{BC}N = 60$. (b) $\chi_{AB}N = \chi_{AC}N = \chi_{BC}N = 75$.

that the saddle point free energies of the LAM_3, KP-PC, and DOHT-PC morphologies are very similar when $f_B > f_C$ and all lower than that of the OOT-PC morphology. However, when $f_B < f_C$, the saddle point free energies of the LAM_3 and KP-PC morphologies are very similar and both lower than that of the DOHT-PC and OOT-PC morphologies. Moreover, for the system with $f_B = f_C$, the LAM_3 and OOT-PC morphologies also have very similar saddle point free energies.

When the volume fraction $f_B = 0.2$, as shown in Fig. 3a, with the volume fraction f_A increasing from 0.2 to 0.4, the ordered micro-phase morphologies change from LAM + C-I to DOHT-PC and finally to OOT-PC morphologies. With the increase of segregation degree, as shown in Fig. 3b, the order–order transition, i.e., from LAM + C-I to LAM + C morphology $[(f_A/f_B/f_C) = (0.2/0.2/0.6)]$, is observed. It should be noted that for the LAM + C morphology, the alternating cylinders formed by the two minority components both have contacts with the lamellae phase domains formed by the majority component, as schematically shown in Fig. 4a. However, for the LAM + C-I morphology, the cylinders inside are surrounded by another minority component and have no contact with the lamellae phase domains formed by the majority component, as schematically shown in Fig. 4b. The saddle point free energies for KP-PC, LAM + C, OOT-PC, DEHT-PC, and DOHT-PC morphologies when the composition $f_A/f_B/f_C$ is 0.3/0.2/0.5 are listed in Table 4. In the intermediate segregation regime, as shown in Table 4, the KP-PC, LAM + C, and OOT-PC morphologies have similar saddle point free energies, which are all higher than that of the DOHT-PC morphology and lower than that of the DEHT-PC morphology. Moreover, when the composition $f_A(f_C)/f_B/f_C(f_A)$ is 0.2/0.2/0.6, an interesting metastable micro-phase morphology, i.e., the SCS + C morphology, is observed, which has not been predicted by 2D studies. In this morphology, the simple-cubic-packed spheres are formed by component B, which connected by the cylinders formed by another minority component along four directions, and the majority component fills the left space. To our knowledge, this micro-phase morphology has not been observed in star block polymer or any other block polymer systems. The SCS + C morphology is found metastable in this work, however, this metastable SCS + C morphology might be stable in the H-shaped (AC)B(CA) ternary block copolymer system with asymmetric interaction parameters.

Near the three edges of these two triangle phase diagrams (Fig. 3a and b), the phase behavior is similar to that of the symmetric linear ABA [38] or four-arm star-like A_2B_2 [39] binary block copolymers because the segregation degree is not strong enough and the mixed phase regions in the micro-phase morphologies are still stable. Furthermore, with the increase of the segregation degree, the order–order transitions from BCC to HPC, from HPC to HPL_2, and from HPL_2 to LAM_2, are observed. In the stable regions of the HPL_2 morphology, two metastable 3D intrinsic micro-phase morphologies, i.e., the *Fddd*L_2 and DL_2 morphologies, are observed. It can be seen that *Fddd*L_2 and DL_2 morphologies are bicontinuous. In this study, the HPL_2 morphology is stable in both weaker and intermediate segregation regimes ($\chi_{AB}N = \chi_{AC}N = \chi_{BC}N = 45$, 60, and 75), which is different from the phase behavior of the binary block

Table 3
The saddle point free energies for LAM_3, KP-PC, OOT-PC, and DOHT-PC morphologies with different compositions when $\chi_{AB}N = \chi_{AC}N = \chi_{BC}N = 75$.

Composition ($f_A/f_B/f_C$)	Saddle point free energy (F/nk_BT)			
	LAM3	KP-PC	OOT-PC	DOHT-PC
0.2/0.5/0.3	−4.189	−4.146	−3.864	−4.171
0.2/0.4/0.4	−5.058		−4.962	
0.2/0.3/0.5	−4.633	−4.595	−4.446	−4.492

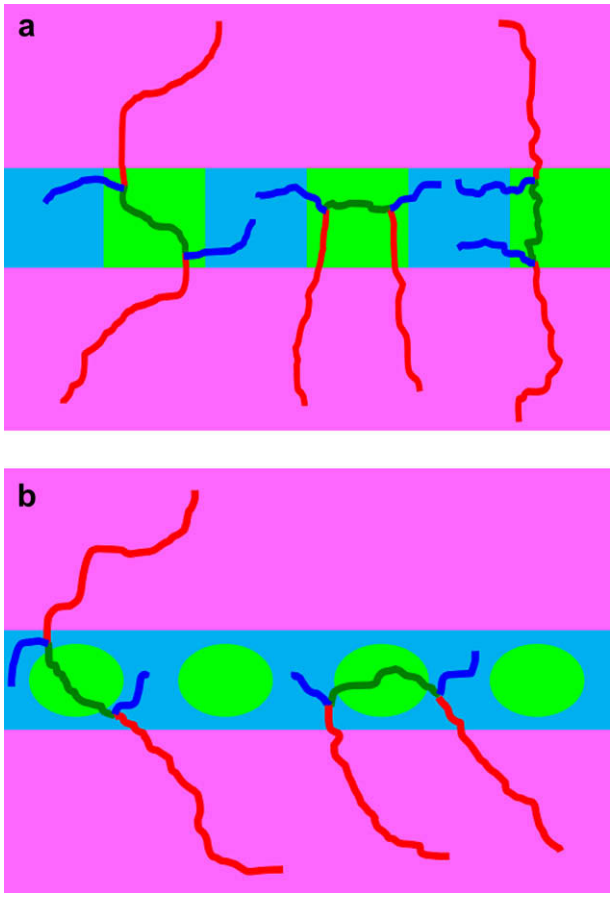

Fig. 4. Schematic representation of the formation of (a) the LAM + C morphology (b) the LAM + C-I morphology when the composition ($f_A/f_B/f_C$) is (0.2/0.2/0.6) in the intermediate segregation regime.

copolymers where the HPL_2 morphology is always metastable [19,44]. This is mainly due to the complex interactions, compositions, and chain architectures of the H-shaped (AC)B(CA) ternary block copolymers. It should be noted that there is only one single diamond phase region in the DL_2 morphology while there are two diamond phase regions in the DD morphology. Moreover, the *Fddd*L_2 and DL_2 morphologies as well as the DG and DD morphologies might exist in a narrow region between the lamellar and hexagonal micro-phase morphologies.

3.3. Strong segregation regime ($\chi_{AB}N = \chi_{AC}N = \chi_{BC}N = 90$, 100, and 125)

As Lee et al. [5,6] have pointed out, for block copolymers with sufficient molecular weight, the phase behavior of the molecules with multiple junction points can be estimated by imaging all bridge and loop blocks to be cut in half. In the strong segregation regime, the phase behavior of this H-shaped (AC)B(CA) ternary block copolymer is similar to that of the three-arm star-like ABC ternary block copolymers. Fig. 5 shows the three-component triangle phase diagrams which cover the whole range of the block copolymer compositions when $\chi_{AB}N = \chi_{AC}N = \chi_{BC}N = 90$, 100, and 125. It should be noted that the triangle phase diagram (Fig. 5b) for $\chi_{AB}N = \chi_{AC}N = \chi_{BC}N = 100$ is the same as that for $\chi_{AB}N = \chi_{AC}N = \chi_{BC}N = 125$. Furthermore, it can be clearly seen that with the increase of the segregation degree, the triangle phase diagram becomes triangularly symmetric.

Near the three edges of these triangle phase diagrams (Fig. 5a and b), the minority component phase-separates from other two majority components due to the increasing interaction energies among the three components. A lot of order–order transitions from "two-color" morphology to "three-color" morphology, such as from HPC to CSHPC, from HPL_2 to HPL_3, and from LAM_2 to LAM_3, are observed. Furthermore, the order–order transition from HPC to HPL_3 is also observed. For the case of the LAM_3 morphology when $f_B = 0.1$, the lamellar widths D_A, D_B, and D_C obey $D_A{:}D_B{:}D_C \approx 2f_A{:}f_B{:}2f_C$. Obviously, this is similar to that of the linear ABC ternary block copolymers [27,34] but different from the LAM_3 morphology of this H-shaped ternary block copolymer in the intermediate segregation regime. In the strong segregation regime, the CS*Fddd*L_3 morphology and the $CSDL_3$ morphology are found as metastable micro-phase morphologies in the stable regions of the CSHPC morphology and the HPL_3 morphology. It should be noted that the CS*Fddd*L_3 and $CSDL_3$ morphologies are tricontinuous, which are similar to the DG and DD morphologies in the binary block copolymers [44,45]. However, the "three-color" core–shell double gyroid phase (CSDG) and the "three-color" core–shell double-diamond phase (CSDD) morphologies, which are pentacontinuous [45], are not found in this study. The stable region of these complex micro-phase morphologies may exist between the CSHPC morphology and the LAM_3 morphology, which is similar to that of the *Fddd*L_2, DL_2, DG, and DD morphologies.

In Fig. 5b ($\chi_{AB}N = \chi_{AC}N = \chi_{BC}N = 100$ and 125), the phase diagram becomes almost triangularly symmetric except individual grid points. When $f_A = f_C$, as the volume fraction f_B increases, the ordered micro-phase morphologies change from LAM_3 to OOT-PC, HEX_3-PC, OHT-PC, LAM + C, and finally to HPC morphologies. This is similar to that of the three-arm star-like ABC ternary block copolymer studied by both MC simulation [46] and the dissipative particle dynamics (DPD) study [47] in the strong segregation regime. In the MC simulation of three-arm star-like ABC ternary block copolymers in the strong segregation regime, when $f_A = f_C$, as the volume fraction f_B increases, the ordered micro-phase morphologies also change from OOT-PC, HEX_3-PC, OHT-PC, and to LAM + C morphologies [46]. However, the decagon-hexagon-tetragon: decagon-octagon-tetragon [10.6.4;10.8.4] (3.3.4.3.4) morphology, which is predicted by both MC simulation [46] and DPD study [47], is not observed in our work. When the volume fraction f_B is large enough, the micro-phase morphologies might terminate with BCC or the close packed sphere phase (CPS) morphologies [48].

When the composition $f_A/f_B/f_C$ is 0.3/0.2/0.5, as shown in Table 4, the DOHT-PC morphology is always the stable micro-phase morphology and its saddle point free energy is lower than that of the KP-PC, LAM + C, DEHT-PC, and OOT-PC morphologies. It can be seen that the saddle point free energies of the KP-PC, LAM + C, DEHT-PC, OOT-PC, and DOHT-PC morphologies have the following sequence: DOHT-PC < OOT-PC < DEHT-PC < LAM + C < KP-PC. This is because that the chain lengths of all the five blocks (A1, C1, B, C2, A2) are almost the same and the distinct blocks tend to separate with each other in the strong segregation regime so that higher

Table 4
The saddle point free energies for KP-PC, LAM + C, OOT-PC, DEHT-PC, and DOHT-PC morphologies with different symmetric interaction parameters when the composition ($f_A/f_B/f_C$) is (0.3/0.2/0.5).

Symmetric interaction parameter χN	Saddle point free energy (F/nk_BT)				
	KP-PC	LAM + C	OOT-PC	DEHT-PC	DOHT-PC
60	−1.831	−1.859	−1.769	−1.687	−1.960
75	−4.192	−4.212	−4.244	−4.116	−4.482
90	−7.027	−7.043	−7.221	−7.049	−7.453
100	−9.122	−9.141	−9.423	−9.221	−9.622
125	−15.032	−15.044	−15.637	−15.364	−15.775

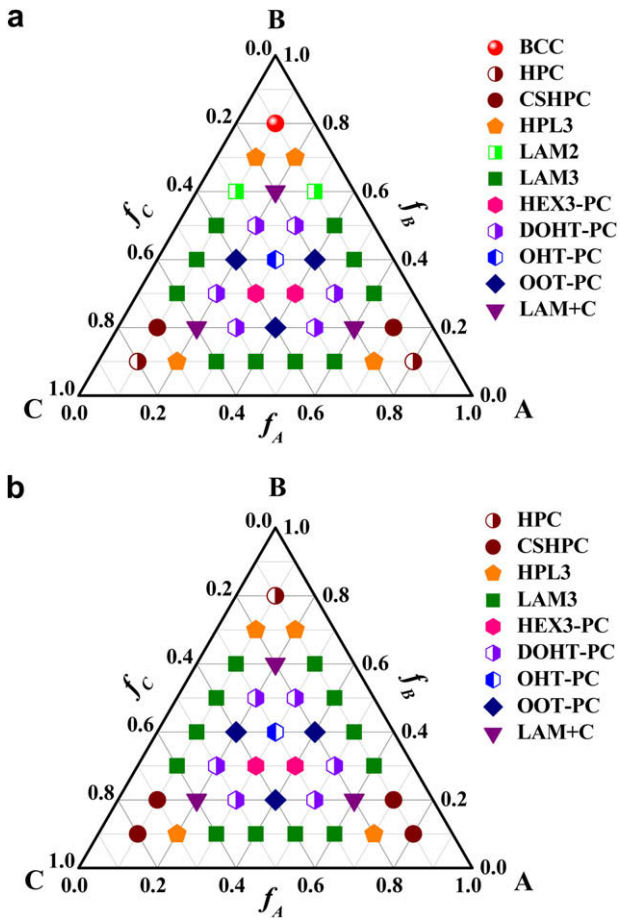

Fig. 5. Triangle phase diagram for the system with (a) $\chi_{AB}N = \chi_{AC}N = \chi_{BC}N = 90$. (b) $\chi_{AB}N = \chi_{AC}N = \chi_{BC}N = 100$ and 125.

curvature of interfaces helps to lower the free energy. When f_A (f_C) = 0.2, as the volume fraction f_B changes from 0.3 to 0.5, the LAM_3 morphology is substituted by the DOHT-PC and OOT-PC morphologies. This is mainly because the stability of the lamellar interfaces decreases with the increase of the segregation degree. The saddle point free energies for LAM_3, KP-PC, OOT-PC, and DOHT-PC morphologies when $f_A/f_B/f_C = 0.2/0.5/0.3$ are listed in Table 5. It can be seen that the saddle point free energy sequence is different from that when $f_A/f_B/f_C$ is 0.3/0.2/0.5 though the DOHT-PC morphology is the most stable structure. This should be attributed that the chain lengths of all the five blocks (A1, C1, B, C2, A2) are almost the same when $f_A/f_B/f_C$ is 0.3/0.2/0.5, while the chain length of block B is much bigger than those of other four blocks (A1, C1, A2, C2) when $f_A/f_B/f_C$ is 0.2/0.5/0.3. When the volume fraction f_B decreases, the stable DOHT-PC morphology occurs in the relatively weak segregation regime. Furthermore, in the strong segregation regime, for the block copolymer with volume fraction of one component is 0.2, if other two components have different volume fractions, the DOHT-PC morphology is the most stable structure, while if other two components have the same volume fraction, the OOT-PC morphology is the most stable structure. This is mainly because that the DOHT-PC morphology and OOT-PC morphology are not very sensitive to the asymmetry of the compositions with equal strong interaction energies among the three components. Moreover, in the strong segregation regime, the metastable HEX_3-PC morphology (data not shown) occurs in the stable region of the OOT-PC morphology, which implies that when the segregation degree becomes strong enough, the OOT-PC morphology can be replaced by the HEX_3-PC morphology.

Table 5
The saddle point free energies for LAM_3, KP-PC, OOT-PC, and DOHT-PC morphologies with different symmetric interaction parameters when the composition ($f_A/f_B/f_C$) is (0.2/0.5/0.3).

Symmetric interaction χN	Saddle point free energy (F/nk_BT)			
	LAM_3	KP-PC	OOT-PC	DOHT-PC
90	−6.688	−6.767	−6.587	−6.942
100	−8.504	−8.727	−8.675	−9.025
125	−13.445	−14.356	−14.717	−14.982

4. Summary

By using a combinatorial screening method based on the self-consistent field theory (SCFT) for polymer systems, the 3D micro-phase morphologies of the H-shaped (AC)B(CA) ternary block copolymers are investigated. Thirteen stable micro-phase morphologies are found, including BCC, HPC, CSHPC, HPL_2, HPL_3, LAM_2, LAM_3, HEX_3-PC, DOHT-PC, OHT-PC, OOT-PC, LAM + C, and LAM + C-I, and seven metastable micro-phase morphologies are also observed, including *Fddd*L_2, DL_2, CS*Fddd*L_3, $CSDL_3$, DEHT-PC, KP-PC, and SCS + C. It is found that in the weaker segregation regime, the minority component can be mixed with other two majority components to form the mixed phase regions. In the intermediate segregation regime, the mixed phase regions phase-separate into three distinct phase regions. Moreover, in the weaker and intermediate segregation regimes, the morphological behavior of this H-shaped (AC)B(CA) ternary block copolymer strongly depends on the bridge connections, which is the key difference from the three-arm star-like ABC ternary block copolymers. In the strong segregation regime, the distinct blocks tend to separate with each other and the effect of the bridge connections on the morphological behavior is close to be negligible so that the phase behavior of this H-shaped (AC)B(CA) ternary block copolymer is similar to that of the three-arm star-like ABC ternary block copolymer. Furthermore, near the three edges of these six triangle phase diagrams the phase behavior of this H-shaped block copolymer is similar to that of the symmetric linear ABA (AB and BC edges) or four-arm star-like A_2B_2 (AC edge) binary block copolymers, while in the center region of these phase diagrams, with the increase of the segregation degree, the curvature of interfaces in the stable micro-phase morphologies increases. These 3D results can help us to design the microstructures of complex block copolymers.

Acknowledgements

The authors appreciate Prof. Chengxiang Zhang (Department of Physics of Jilin University) for the fruitful comments and helpful discussions. This work is supported by the National Natural Science Foundation of China (50873098, 20620120105, 20534020, and 20734006), Programs and the Fund for Creative Research Groups (50621302). The authors also appreciate the financial support of JLSTP (20070113).

References

[1] Hamley IW. The physics of block copolymers. New York: Oxford University Press; 1998.
[2] Sato T, Hasko DG, Ahmed H. Journal of Vacuum Science and Technology B 1997;15:45.
[3] Böltau M, Walheim S, Mlynek J, Krausch G, Steiner U. Nature 1998;391:877.
[4] Srinivasarao M, Collings D, Philips A, Patel S. Science 2001;292:79.
[5] Lee C, Gido SP, Poulos Y, Hadjichristidis N, Tan NB, Trevino SF, et al. Polymer 1998;39:4631.
[6] Lee C, Gido SP, Poulos Y, Hadjichristidis N, Tan NB, Trevino SF, et al. Journal of Chemical Physics 1997;107:6460.
[7] Yu XF, Shi TF, Zhang G, An LJ. Polymer 2006;47:1538.
[8] Xu K, Wang Y, Wang YX, Yu T, An LJ, Pan CY, et al. Polymer 2006;47:4480.

[9] Yu XF, Zhang G, Shi TF, Han YC, An LJ. Polymer 2007;48:2489.
[10] Han DH, Pan CY. Journal of Polymer Science, Part A: Polymer Chemistry 2007;45:789.
[11] Mijovic J, Sun MY, Pejanovic S, Mays JW. Macromolecules 2003;36:7640.
[12] Li AX, Lu ZJ, Zhou QF, Qiu F, Yang YL. Journal of Polymer Science, Part A: Polymer Chemistry 2006;44:3942.
[13] Gu LN, Shen Z, Zhang S, Lu GL, Zhang XH, Huang XY. Macromolecules 2007;40:4486.
[14] Blencowe A, Tan JF, Goh TK, Qiao GG. Polymer 2009;50:5.
[15] Edwards SF. Proceedings of the Physical Society 1965;85:613.
[16] Leibler L. Macromolecules 1980;13:1602.
[17] Semenov AN. Soviet Physics JETP 1985;61:733.
[18] Helfand E, Wasserman ZR. Macromolecules 1980;13:994.
[19] Matsen MW, Schick M. Physical Review Letters 1994;72:2660.
[20] Matsen MW. Physical Review Letters 1998;80:4470.
[21] Drolet F, Fredrickson GH. Physical Review Letters 1999;83:4317.
[22] Drolet F, Fredrickson GH. Macromolecules 2001;34:5317.
[23] Fredrickson GH, Ganesan V, Drolet F. Macromolecules 2002;35:16.
[24] Tzeremes G, Rasmussen KØ, Lookman T, Saxena A. Physical Review E 2002;65:041806.
[25] Sides SW, Fredrickson GH. Polymer 2003;44:5859.
[26] Guo ZJ, Zhang GJ, Qiu F, Zhang HD, Yang YL, Shi AC. Physical Review Letters 2008;101:028301.
[27] Tang P, Qiu F, Zhang HD, Yang YL. Physical Review E 2004;69:031803.
[28] Tang P, Qiu F, Zhang HD, Yang YL. Journal of Physical Chemistry B 2004;108:8434.
[29] Ye XG, Shi TF, Lu ZY, Zhang CX, Sun ZY, An LJ. Macromolecules 2005;38:8853.
[30] Ye XG, Yu XF, Sun ZY, An LJ. Journal of Physical Chemistry B 2006;110:12042.
[31] Ye XG, Yu XF, Shi TF, Sun ZY, An LJ, Tong Z. Journal of Physical Chemistry B 2006;110:23578.
[32] Wang R, Hu JL, Jiang ZB, Zhou DS. Macromolecular Theory and Simulations 2005;14:256.
[33] Wang R, Xu TT. Polymer 2007;48:4601.
[34] Sun MZ, Wang P, Qiu F, Tang P, Zhang HD, Yang YL. Physical Review E 2008;77:016701.
[35] Thomas JW. Numerical partial differential equations. New York: Springer; 1995.
[36] Press WH, Teukolsky SA, Vetterling WT, Flannery BP. Numerical recipes. Cambridge: Cambridge University Press; 1989.
[37] He XH, Liang HJ, Huang L, Pan CY. Journal of Physical Chemistry B 2004;108:1731.
[38] Matsen MW, Thompson RB. Journal of Chemical Physics 1999;111:7139.
[39] Matsen MW, Gardiner JM. Journal of Chemical Physics 2000;113:1673.
[40] Gemma T, Hatano A, Dotera T. Macromolecules 2002;35:3225.
[41] Dotera T, Hatano A. Journal of Chemical Physics 1996;105:8413.
[42] He XH, Huang L, Liang HJ, Pan CY. Journal of Chemical Physics 2003;118:9861.
[43] Bohbot-Raviv Y, Wang Z-G. Physical Review Letters 2000;85:3428.
[44] Matsen MW. Journal of Physics: Condensed Matter 2002;14:R21.
[45] Shefelbine TA, Vigild ME, Matsen MW, Hajduk DA, Hillmyer MA, Cussler EL, et al. Journal of the American Chemical Society 1999;121:8457.
[46] Ueda K, Dotera T, Gemma T. Physical Review B 2007;75:195122.
[47] Huang CI, Fang HK, Lin CH. Physical Review E 2008;77:031804.
[48] Matsen MW, Bates FS. Macromolecules 1996;29:1091.